Proceedings of the Thirty-sixth (2026) International Ocean and Polar Engineering Conference **www.isope.org**
Orlando, Florida, USA, May 31-June 5, 2026

ISBN 978-1-880653-72-2; ISSN 1098-6189

Numerical Investigation of a KCS Ship Berthing and Unberthing Based on the Overset Grid Method

Sinian Li, Zhihao Wang, Jianhua Wang, Decheng Wan[*]

Computational Marine Hydrodynamics Lab (CMHL), School of Ocean and Civil Engineering.
Shanghai Jiao Tong University, Shanghai, China
[*]Corresponding Author

ABSTRACT.

The increasing scale of modern ports, coupled with complex bathymetry and dynamic hydrological conditions, presents significant challenges to ship berthing and unberthing operations. In this study, overset grid is performed using the open-source OpenFOAM platform with Suggar++. The solver uses naoe-FOAM-SJTU developed within the group. The forces and moments acting on the KCS hull during berthing and unberthing maneuvers under a uniform inflow condition are numerically investigated. This study investigates the effects of four key factors—berthing and unberthing velocity, uniform inflow velocity, ship heading angle, and water depth—on the forces and moments acting on the KCS hull, incorporating complex topography in the numerical simulations. The results demonstrate that increased ship speed, inflow velocity, and heading angle, or reduced water depth augment the lateral force and moment of turning ship, thereby increasing the risk of bow collision with the quay wall. These findings contribute to defining the safe operational envelope for berthing and unberthing and provide a valuable reference for practical engineering applications.

KEY WORDS: overset grid; naoe-FOAM-SJTU; berthing and unberthing; lateral force; moment of turning ship

INTRODUCTION

Berthing and unberthing are among the most complex and highest-risk procedures in port operations. With the development of the global shipping industry, the trend toward vessel gigantism—such as ultra-large container ships and large cruise ships—has become increasingly evident, posing unprecedented challenges to the safety and efficiency of port operations. The berthing and unberthing process involves complex interactions among vessels, port facilities, and the environment, where any operational error may lead to collisions, groundings, or damage to docks, resulting in significant economic losses and safety incidents. According to statistics (Zhang, Wu, Liu, He and Li, 2023), nearly 70% of port accidents are related to human error during berthing and unberthing operations. Therefore, achieving safe, precise, and efficient berthing and unberthing has become a core issue in the intelligent transformation of the shipping industry. However, the hydrodynamic forces acting on large container ships at extremely low speeds exhibit pronounced nonlinear and coupled characteristics. Traditional empirical formulas based on constant-speed domains or simplified mathematical models often struggle to provide accurate predictions. In particular, the complex vortex fields generated by the close-range interactions between the hull and the quay wall or seabed cause drastic variations in the lateral forces and yaw moments on the vessel, posing a significant threat to maneuvering safety.

Computational Fluid Dynamics (CFD) numerical simulation offers a powerful tool to address this challenge. It enables high-resolution analysis of the viscous flow field around the hull and captures vortex structures, allowing for refined prediction of ship hydrodynamics without the need for costly physical experiments. In recent years, researchers have begun utilizing CFD to analyze specific scenarios such as bank effects and lateral motions, and have compared the predictive performance of different low-speed ship force models. These efforts lay a solid foundation for further in-depth research. Toda, Lee, and SADAKANE (2002), by employing a method combining CFD numerical simulations with towing experiment validation, proposed the hydrodynamic forces during berthing exhibit significant transient and transitional features, primarily dominated by pressure components, and the generation and evolution of vortices substantially influence these forces. Sasa, Kubo, Nagai, Yoneyama, and Shiraishi (2005) constructed numerical simulations of ship motions in swells during harbor entrance and departure and therefore proposed and verified as the Difficulty of Berthing Function, which can evaluate the operational difficulty quantitatively.

In addition, as ship berthing and unberthing operations are considered the most complex operational procedures, requiring vessels to navigate safely under high-pressure conditions, the issue of safe berthing and unberthing has attracted increasing attention. Bui, Kawai, Kim, and Lee (2011) proposed a new approach for ship berthing with the assistance of autonomous tugboats The efficiency of the proposed approach was evaluated through using a model ship in a Matlab simulation. It exhibited good performance and revealed the possibility of extending these results to future studies by testing a model ship under actual conditions. Abramowicz-Gerigk and Jachowski.(2022) determined the relationship between the pressure on the quay wall and flow velocity on the seabed using real-scale CFD simulation of the flow field generated during berthing and unberthing maneuvers. Okuda, Yasukawa, Hirata, and Matsuda employed a combination of free-running model tests and numerical simulations to investigate the berthing and unberthing performance of a single-propeller, single-rudder ship equipped with a bow thruster. By proposing and validating the "oblique sailing navigation (OSN) method," they demonstrated that the ship can safely berth and unberth under the condition of a water depth-to-draft ratio of h/d = 1.5. Mwange, Miyauchi, Kambara, Koike, Hosogaya, Ishibashi, and Maki (2025) employed statistical analysis based on one-year operational data from a full-scale ship to quantitatively investigate the berthing and unberthing maneuvering characteristics of a coastal vessel equipped with a Vectwin rudder system and a bow thruster across multiple ports, providing key quantitative insights for improving low-speed maneuvering models, optimizing captive model test conditions, and developing autonomous berthing/unberthing algorithms and digital twins.

To sum up, ship berthing and unberthing operations present a critically important and complex problem. This study conducts numerical simulations of the berthing and unberthing maneuvers of a KCS hull using the open-source OpenFOAM platform with Suggar++ (Noack, Boger, Kunz, and Carrica, 2009), with the solver naoe-FOAM-SJTU. Overset grid techniques are employed to investigate the forces and moments acting on the KCS hull during these maneuvers under uniform inflow conditions. The effects of four key factors—ship speed during berthing and unberthing, uniform inflow velocity, ship heading angle, and water depth—on the hydrodynamic forces and moments are systematically analyzed, with complex topography incorporated into the numerical simulations. The findings contribute to defining the safe operational envelope for berthing and unberthing and provide a valuable reference for practical engineering applications.

NUMERICAL METHOD

naoe-FOAM-SJTU Solver

The naoe-FOAM-SJTU solver is a CFD numerical tool developed for hydrodynamics in naval architecture and ocean engineering, based on the open-source code OpenFOAM-3.0.0. This solver is capable of handling dynamic overset grids and features a multi-body six-degree-of-freedom motion module developed specifically for the overset grid method, which enables the simulation of complex problems such as the interaction and motion coupling between the ship hull, propeller, and rudder. The Dynamic Cell Interpolation (DCI) generated by the overset grid interpolation program Suggar++ is adopted to accomplish the flow-field communication and solution between overset grids.

Governing Equations

The flow is treated as viscous, unsteady, and incompressible. The controlling equations are formulated using the Reynolds-averaged Navier–Stokes (RANS) equations, given as:

$$\frac{\partial u_i}{\partial x_i} = 0 \tag{1}$$

$$\frac{\partial u_i}{\partial t} + \frac{\partial}{\partial x_j}\left(u_i u_j\right) = -\frac{1}{\rho}\frac{\partial p}{\partial x_i} + \nu\frac{\partial}{\partial x_j}\left[\frac{\partial u_i}{\partial x_j} + \frac{\partial u_j}{\partial x_i}\right] \tag{2}$$

where u_i (i = 1, 2, 3) is the velocity component in the direction of the three axes of x, y, and z; x_i (i = 1, 2, 3) is the coordinate component in the direction of the three axes of x, y, and z. p is the pressure of the fluid; ρ is the density of the fluid; ν is the kinematic viscosity coefficient of the fluid; t is the time. For the turbulence model, k-ω SST, introduced by Menter(1994), is chosen for the calculation.

To precisely track the free surface as the containership moves through water, the Volume of Fluid (VOF) approach is employed to limit numerical diffusion. The corresponding equations are:

$$\frac{\partial \alpha}{\partial t} + \nabla \cdot [(U - U_g)\alpha] + \nabla \cdot [U_r(1-\alpha)\alpha] = 0 \tag{3}$$

Where α is the volume fraction and $0<\alpha<1$. The volume fraction α can be expressed as:

$$\alpha = \begin{cases} 0 & \text{air} \\ 1 & \text{water} \end{cases} \tag{4}$$

At the same time, the fluid density ρ and the coefficient of dynamic viscosity μ_{eff} can also be expressed by α.

$$\rho = \alpha\rho_1 + (1-\alpha)\rho_g \tag{5}$$

$$\mu = \alpha\mu_1 + (1-\alpha)\mu_g \tag{6}$$

where the ρ_l and μ_l represent the density and dynamic viscosity of water, the ρ_g and μ_g represent the density and dynamic viscosity of air.

Ship Motion

The six-degree-of-freedom (6DOF) module integrated into the naoe-FOAM-SJTU solver is employed to simulate ship motion under wave conditions. This 6DOF framework decomposes vessel movement into three translational modes—surge, sway, and heave—and three rotational modes—roll, pitch, and yaw. To enable the solution of these motions, two coordinate systems are defined: a fixed geodetic (earth) coordinate system and a hull-fixed coordinate system. The geodetic system remains stationary, while the hull system moves with the ship, with its origin typically positioned at the center of gravity. For clarity, the axes of the hull system are oriented such that the X-axis aligns with the ship’s longitudinal direction, the Y-axis with its transverse (width) direction, and the Z-axis with the vertical (draft) direction. When the ship is in an upright floating condition, the positive directions of the hull coordinate axes coincide with those of the geodetic system.

The ship’s motion as observed in the geodetic frame is essentially the relative movement of the hull coordinate system with respect to the geodetic system. Consequently, the displacement of the ship in the geodetic frame can be expressed as:

$$\boldsymbol{\eta} = (\boldsymbol{\eta}_1, \boldsymbol{\eta}_2) = (x, y, z, \phi, \theta, \psi) \tag{7}$$

Here, the six parameters represent the translational displacements along the X, Y, and Z axes (surge, sway, heave) and the angular displacements about these axes (roll, pitch, yaw). The corresponding linear and angular velocities are defined within the hull coordinate system:

$$v = (v_1, v_2) = (u, v, w, p, q, r) \tag{8}$$

The relationship between the velocities in the geodetic and hull coordinate systems is established using the three Euler angles that describe the ship's orientation:

$$\boldsymbol{v}_1=\boldsymbol{J}_1^{-1}\cdot\dot{\boldsymbol{\eta}}_1,\quad \boldsymbol{v}_2=\boldsymbol{J}_2^{-1}\cdot\dot{\boldsymbol{\eta}}_1,\qquad \dot{\boldsymbol{\eta}}_1=\boldsymbol{J}_1\cdot\boldsymbol{v}_1,\quad \dot{\boldsymbol{\eta}}_1=\boldsymbol{J}_2\cdot\boldsymbol{v}_2 \tag{9}$$

where J_1 and J_2 are conversion matrices with the following expressions.

$$\boldsymbol{J}_1=\begin{bmatrix}\cos\theta\cos\psi & \sin\phi\sin\theta\cos\psi-\cos\phi\sin\psi & \cos\phi\sin\theta\cos\psi+\sin\phi\sin\psi\\ \cos\theta\sin\psi & \sin\phi\sin\theta\sin\psi+\cos\phi\cos\psi & \cos\phi\sin\theta\sin\psi-\sin\phi\cos\psi\\ -\sin\theta & \sin\phi\cos\theta & \cos\phi\cos\theta\end{bmatrix} \tag{10}$$

$$\boldsymbol{J}_2=\begin{bmatrix}1 & \sin\phi\tan\theta & \cos\phi\tan\theta\\ 0 & \cos\phi & -\sin\phi\\ 0 & \dfrac{\sin\phi}{\cos\theta} & \dfrac{\cos\phi}{\cos\theta}\end{bmatrix} \tag{11}$$

GEOMETRY AND WORKING CONDITION DESIGN

Geometric Model

The 20,000 TEU ultra-large container ship is a hydroelastic test benchmark model used by the China Ship Scientific Research Center in the international Joint Industry Project (JIP) (Yang, Feng, Chen, and Wen, 2021). The geometry model of the containership is shown in Fig. 1, and the figure containership's principal dimensions in model scale are provided in Table 1.

Fig 1. Geometry model of the KCS

Table 1. Main particulars of the KCS

Particulars	Symbols and units	Value
Length between perpendiculars	L(m)	383.0
Total width	B(m)	58.6
Fore Draft	T_1(m)	15.2
Aft Draft	T_2(m)	16.7
Depth	D(m)	22.5
Displacement	∇(ton)	2.58×10^5

Computational Domain Setting and Grid Independence

The computing domain and boundary conditions applied for the flow field distribution simulations are presented in Fig. 2. The dimensions of the computing domain were 690 m × 230 m × 32 m.

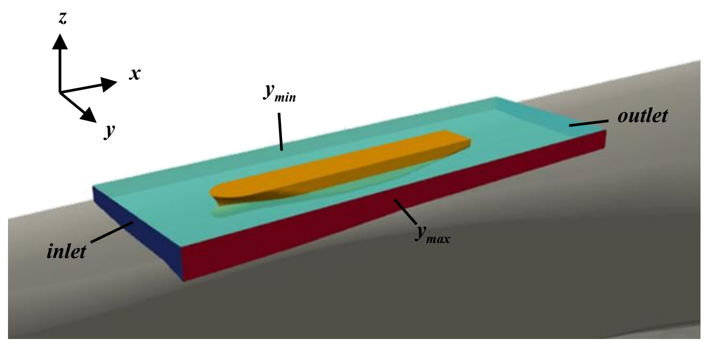

Fig 2. The computational domain

The grid setting is mainly composed of two parts, namely the overset grid area and the background grid area. The meshing diagram is shown in Fig. 3. Among them, the inner area of the blue frame is the overlapping grid area, and the outer area of the red frame is the background grid area.

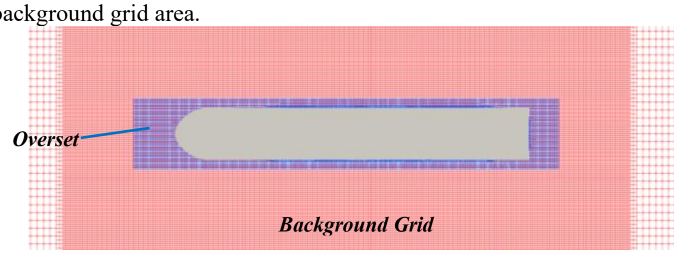

Fig 3. Illustration of grid arrangement

Following a refinement ratio of $\sqrt{2}$, with the grid cell count in each direction increasing by a factor of $\sqrt[6]{2}$, three sets of systematically refined grids of 2.70 million (coarse), 4.01 million (medium), and 5.30 million (fine) were constructed to simulate the berthing of the KCS at a speed of 1 m/s. The lateral forces and yaw moments during berthing were compared in Fig. 4 and Fig. 5. The time histories of lateral force and yaw moment show good agreement between the medium and fine grids, while the coarse grid exhibits noticeable oscillations, indicating that a grid resolution of at least 4.01 million cells is required for stable and accurate predictions. Therefore, to ensure both computational efficiency and quality, a medium grid size was selected for subsequent calculations.

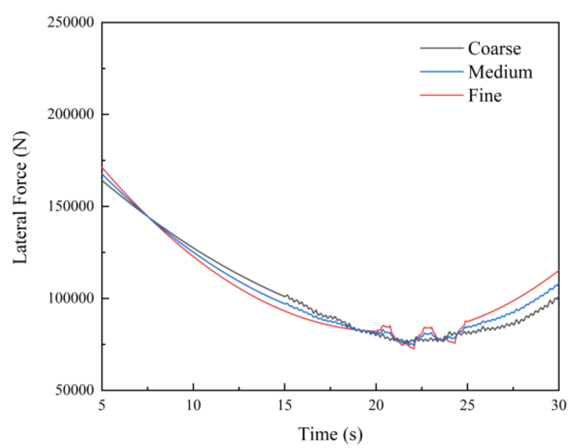

Fig 4. Time history curve of the lateral force for three grid sets

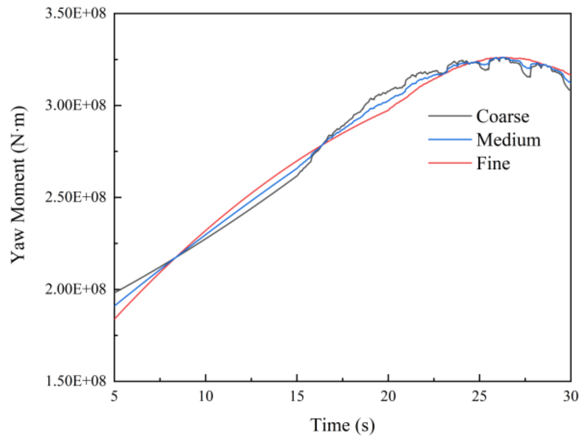

Fig 5. Time history curve of the yaw moment for three grid sets

CALCULATION CONDITION SETTING

Taking berthing/unberthing speed, water depth, ship heading angle, and inflow velocity as variables, a total of 18 scenarios were designed for both the berthing and unberthing maneuvers of the KCS hull in Table 2 and Table 3.

Table 2. Design of berthing conditions

Calculation conditions	Berthing speed	Inflow velocity	Water depth
1	3cm/s	(0.1, 0, 0)m/s	20m
2	4cm/s	(0.1, 0, 0)m/s	20m
3	5cm/s	(0.1, 0, 0)m/s	20m
4	5cm/s	(0.1, 0, 0)m/s	25m
5	5cm/s	(0.1, 0, 0)m/s	30m
6	5cm/s	(0.087, 0.05, 0)m/s	20m
7	5cm/s	(0.0707, 0.0707, 0)m/s	20m
8	5cm/s	(0.05, 0.087, 0)m/s	20m
9	5cm/s	(0.15, 0, 0)m/s	20m

Table 3. Design of unberthing conditions

Calculation conditions	Unberthing speed	Inflow velocity	Water depth
1	3cm/s	(0.1, 0, 0)m/s	20m
2	4cm/s	(0.1, 0, 0)m/s	20m
3	5cm/s	(0.1, 0, 0)m/s	20m
4	5cm/s	(0.1, 0, 0)m/s	25m
5	5cm/s	(0.1, 0, 0)m/s	30m
6	5cm/s	(0.087, 0.05, 0)m/s	20m
7	5cm/s	(0.0707, 0.0707, 0)m/s	20m
8	5cm/s	(0.05, 0.087, 0)m/s	20m
9	5cm/s	(0.15, 0, 0)m/s	20m

Time histories of the surge force X, lateral force Y, and yaw moment N acting on the ship were extracted to analyze the influence of these four variables on the forces and moments during low-speed port entry and departure operations.

RESULT AND DISCUSSION

Flow Field Analysis

Fig. 6 and Fig. 7 respectively present the computational results for the KCS hull during berthing under a 45° oblique current and unberthing under a straight current, showing velocity cloud diagram at 20s, 30s, and 40s. It can be observed that during berthing, as the hull gradually approaches the quay, the flow in the gap between the hull and the quay accelerates, forming a localized high-velocity region. Throughout the motion, a distinct high-velocity zone consistently appears at the bow, while a low-velocity zone forms at the stern. This asymmetric flow field distribution is the primary reason for the hull experiencing significant lateral force and yaw moment, thereby increasing the risk of stern collision with the quay wall. For unberthing, similarly, the asymmetric flow field distribution raises the risk of bow collision with the quay.

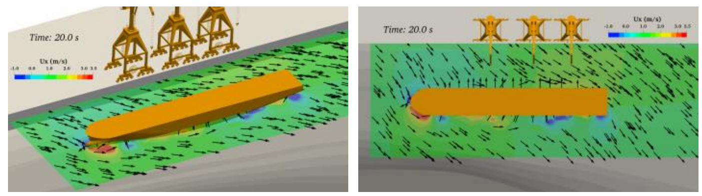

(a) When Time = 20.0s, berthing speed = 5cm/s and inflow velocity = (0.0707 , 0.0707 , 0)m/s, the velocity cloud diagram is shown

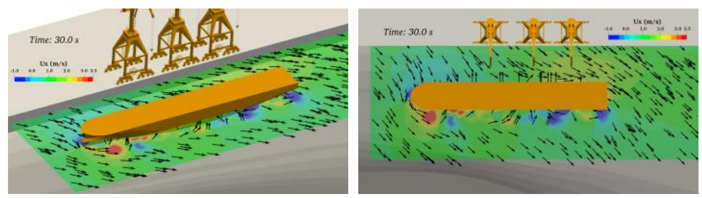

(b) When Time = 30.0s, berthing speed = 5cm/s and inflow velocity = (0.0707 , 0.0707 , 0)m/s, the velocity cloud diagram is shown

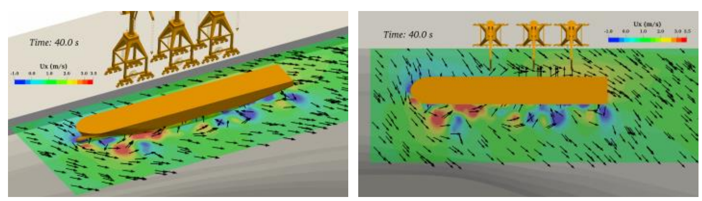

(c) When Time = 40.0s, berthing speed = 5cm/s and inflow velocity = (0.0707 , 0.0707 , 0)m/s, the velocity cloud diagram is shown

Fig 6. Velocity cloud diagram for the KCS during berthing under berthing speed = 5cm/s and inflow velocity = (0.0707 , 0.0707 , 0)m/s

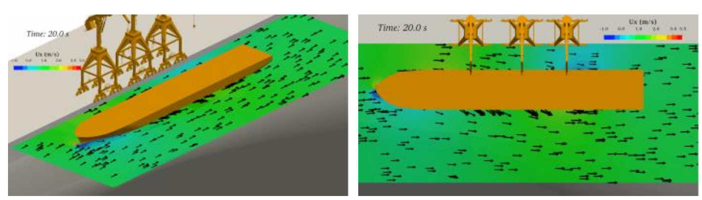

(a) When Time = 20.0s, unberthing speed = 5cm/s and inflow velocity = (0.1 , 0 , 0)m/s, the velocity cloud diagram is shown

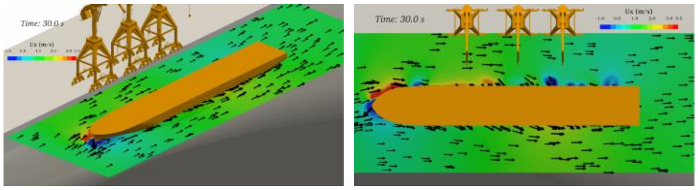

(b) When Time = 30.0s, unberthing speed = 5cm/s and inflow velocity = (0.1 , 0 , 0)m/s, the velocity cloud diagram is shown

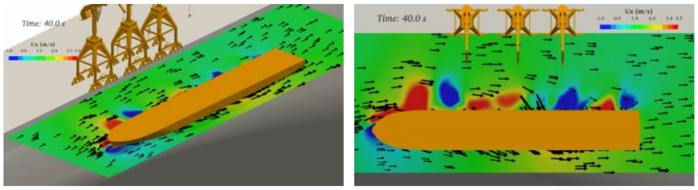

(c) When Time = 40.0s, unberthing speed = 5cm/s and inflow velocity = (0.1 , 0 , 0)m/s, the velocity cloud diagram is shown

Fig 7. Velocity cloud diagram for the KCS during unberthing under unberthing speed = 5cm/s and inflow velocity = (0.1 , 0 , 0)m/s

Berthing and Unberthing Speed

Figs. 8~9 present the time histories of the forces and moments acting on the KCS hull under different berthing and unberthing speeds. Under identical uniform inflow conditions, the surge force X is less sensitive to variations in ship speed, whereas the lateral force Y is significantly influenced by ship speed. As the maneuver progresses, the surge force X exhibits a decreasing trend, while the lateral force Y tends to increase over time. Under the same inflow velocity, the yaw moment N increases substantially with increasing berthing or unberthing speed. During berthing, a positive yaw moment is induced, elevating the risk of stern collision with the quay wall. Conversely, during unberthing, a negative yaw moment is generated, making the bow more susceptible to collision with the quay.

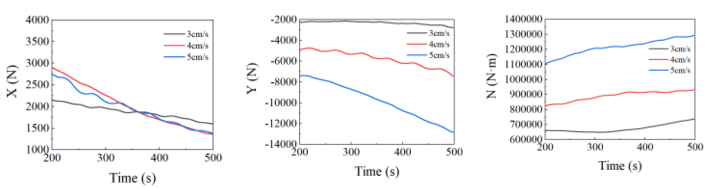

(a)X (b)Y (c)N

Fig 8. Time history data under berthing conditions at different berthing speeds

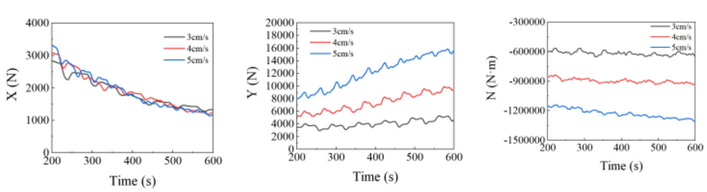

(a)X (b)Y (c)N

Fig 9. Time history data under unberthing conditions at different unberthing speeds

Water Depth

Figs. 10~11 present the time histories of the forces and moments acting on the KCS hull berthing and unberthing under different water depths. At a water depth of 20 m, the shallow water effect becomes pronounced, resulting in significantly larger forces compared to those at greater depths. The forces also exhibit more pronounced fluctuations due to intensified hydrodynamic interactions. The yaw moment experienced by the ship increases markedly at 20 m depth relative to that at 25 m and 30 m depths, indicating that reduced under-keel clearance amplifies the turning tendency during maneuvers.

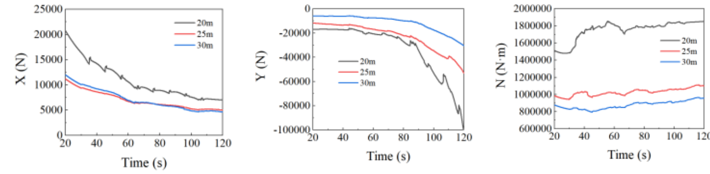

(a)X (b)Y (c)N

Fig 10. Time history data under berthing conditions at different water depths

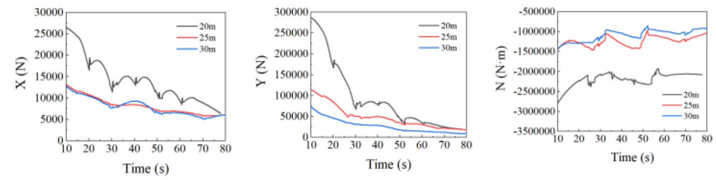

(a)X (b)Y (c)N

Fig 11. Time history data under unberthing conditions at different water depths

Ship Heading Angle

Figs. 12~13 present the time histories of the forces and moments acting on the KCS hull berthing and unberthing under different ship heading angles. When the inflow angle is 30°, the transverse component of the inflow aligns with the ship's berthing motion, creating a quasi-steady relative condition in the lateral direction. This results in nearly zero lateral force Y. Correspondingly, the yaw moment N also approaches zero at this angle due to the absence of significant transverse flow asymmetry. As the inflow angle increases, the asymmetry intensifies, leading to a progressive increase in the yaw moment acting on the hull. For unberthing conditions, as the inflow angle increases, the surge force X decreases, the lateral force Y increases, and the yaw moment acting on the ship also increases.

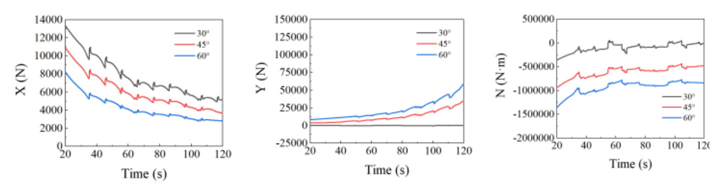

(a)X (b)Y (c)N

Fig 12. Time history data under berthing conditions at different ship heading angles

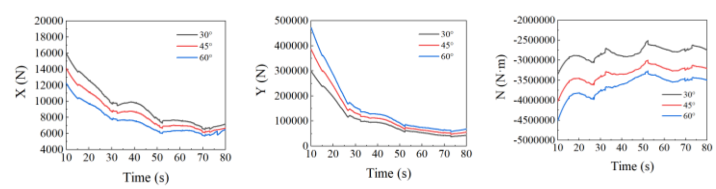

(a)X (b)Y (c)N

Fig 13. Time history data under unberthing conditions at different ship heading angles

Inflow Velocity

Figs. 14~15 present the time histories of the forces and moments acting on the KCS hull berthing and unberthing under different inflow velocities. At higher inflow velocities, the surge force X and yaw moment N increase significantly. Since the flow velocity varies only in the x-direction, the lateral force Y is less affected by changes in inflow velocity. For berthing conditions, as the distance to the quay wall decreases, the flow velocity near the wall is lower than that in the channel, which diminishes the influence of different inflow velocities on the surge force X, causing the X-force values under various inflow velocities to converge. For unberthing conditions, a larger negative yaw moment is induced at higher inflow velocities, increasing the likelihood of bow collision with the quay wall.

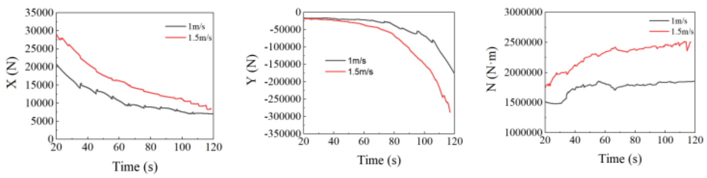

(a)X (b)Y (c)N

Fig 14. Time history data under berthing conditions at different inflow velocities

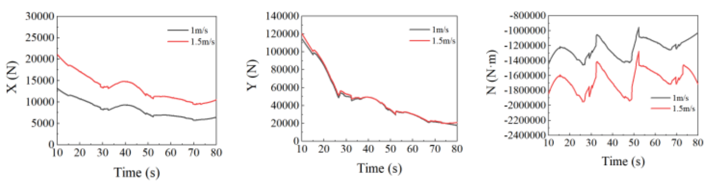

(a)X (b)Y (c)N

Fig 15. Time history data under unberthing conditions at different inflow velocities

CONCLUSIONS

In this study, the berthing and unberthing maneuvers of a KCS hull are numerically investigated using the overset grid method within the OpenFOAM framework coupled with the naoe-FOAM-SJTU solver. A series of numerical simulations were conducted to systematically analyze the effects of four key parameters—berthing and unberthing speed, water depth, ship heading angle, and inflow velocity—on the hydrodynamic forces (surge force X, lateral force Y) and yaw moment N acting on the hull. The flow field analysis reveals a distinct asymmetry during berthing and unberthing. As the hull approaches the quay, the gap flow accelerates, creating a persistent high-velocity zone at the bow and a low-velocity zone at the stern. This asymmetric distribution is the primary cause of the significant lateral force and yaw moment, which directly correlate with collision risk. The findings quantitatively demonstrate that increased ship speed, inflow velocity, and heading angle, or reduced water depth, all contribute to larger lateral forces and yaw moments, thereby elevating collision risks during berthing and unberthing. This study provides quantitative insights for defining safe operational envelopes and offers a reliable reference for practical engineering applications and the development of autonomous maneuvering algorithms.

ACKNOWLEDGEMENTS

This work is supported by the National Natural Science Foundation of China (52131102), to which the authors are most grateful.

REFERENCES

Abramowicz-Gerigk, T, and Jachowski, J.(2022). “Ship Berthing and Unberthing Monitoring System in the Ferry Terminal,” *Sensors*, 22(23): 9133.

Bui, VP., Kawai, H., Kim, YB., and Lee, KS.(2011). “A ship berthing system design with four tug boats,” *Journal of mechanical science and technology*, 25(5): 1257-1264.

Menter, FR (1994). “Two-equation eddy-viscosity turbulence models for engineering applications,” *AIAA J*, 32(8), 1598–1605.

Mwange, AN, Miyauchi, Y, Kambara, T, Koike, H, Hosogaya, K, Ishibashi, A, and Maki, A.(2025). “Quantitative evaluation of full-scale ship maneuvering characteristics during berthing and unberthing,” *Journal of Marine Science and Technology*, 1-23.

Noack, R, Boger, D, Kunz, R, and Carrica, P (2009). “Suggar++: An improved general overset grid assembly capability,” *19th AIAA Computational Fluid Dynamics*, 2009: 3992.

Okuda, R, Yasukawa, H, Hirata, N, and Matsuda, A.(2024). “A study on berthing and unberthing of a single-shaft ship with a bow thruster,” *Journal of Marine Science and Technology*, 29(1): 53-74.

Sasa, K., Kubo, M., Nagai, T., Yoneyama, H., and Shiraishi, S (2005). “A study of difficulties of entering and departing harbours due to wave-induced ship motions,” *Proc 17th Int Offshore and Polar Eng Conf*, Lisbon, ISOPE, 3, 1880–1888.

Toda, Y, Lee, YS, and SADAKANE, H (2002). “Numerical investigations of hydrodynamic forces acting on a ship hull under lateral low speed motion,” *Journal of the Kansai Society of Naval Architects*, Japan, 2002(238), 238_77–238_83.

Yang, P, Feng, QD, Chen, HS, and Wen, LJ (2021). “Combined backbone application on numerical simulations and a model experiment of a 20,000 TEU container ship,” *Ocean Engineering*, 223: 108662.

Zhang, S, Wu, Q, Liu, JL, He, YY, and Li, SJ (2023). “State-of-the-Art Review and Future Perspectives on Maneuvering Modeling for Automatic Ship Berthing,” *Journal of Marine Science and Engineering*, 11(9): 1824